Supplemental Information

ISWI remodelers slide nucleosomes with coordinated multi-base-pair entry steps and single-base-pair exit steps

Sebastian Deindl, William L. Hwang, Swetansu K. Hota, Timothy R. Blosser, Punit Prasad, Blaine Bartholomew, and Xiaowei Zhuang

Supplemental Information Contents:

Figure S1. The FRET distributions of exit-side-labeled nucleosomes before and after remodeling by ISW2 and dependence of FRET on the exit linker DNA length, related to Figure 1.

(A) Left: The initial FRET distribution of the n = 3 bp nucleosomes before addition of enzyme. The FRET histogram (blue bars) displays three peaks centered at FRET = 0.87, 0.49 and 0.70 (derived from a Gaussian fit, black line) that result from the three distinct donor-labeling configurations, with 1) a single donor dye on the H2A subunit proximal to the acceptor dye on the DNA, 2) a single donor dye on the H2A subunit distal to the acceptor dye on the DNA, or 3) two donor dyes (one on each H2A subunit), respectively. This assignment was further confirmed by fluorescence time traces, which showed a single donor-photobleaching step for the high and low FRET peaks, and two donor-photobleaching steps for the intermediate FRET peak.

Middle: The FRET distributions of the n = 3 bp nucleosomes upon addition of ISW2 alone (red line) or upon addition of both ISW2 and ATP (black shaded bars) superimposed on the initial FRET histogram (blue bars).

Right: The FRET distributions of the n = 3 bp nucleosomes after removal of the population with two donor dyes. This nucleosome population was removed by eliminating FRET traces with two donor-photobleaching steps. As expected, the middle peak in the pre-remodeling FRET distributions disappeared. Blue bars: initial FRET distribution; red line: FRET distribution after addition of ISWI2 alone. Black shaded bars: FRET distribution upon addition of both ISW2 and ATP.

(B) The FRET distributions of the n = -3 bp nucleosomes in the absence of ISW2 (blue bars), in the presence of ISW2 alone (red line), and upon addition of both ISW2 and ATP (black shaded

bars). The nucleosome population with two donor dyes was removed by eliminating FRET traces with two donor-photobleaching steps.

(C) The FRET distributions of the m = 10 bp nucleosomes in the absence of ISW2 (blue bars), in the presence of ISW2 alone (red line), and upon addition of both ISW2 and ATP (black shaded bars). The nucleosome population with two donor dyes was removed by eliminating FRET traces with two donor-photobleaching steps.

(D) FRET values for a series of nucleosome constructs with different linker DNA lengths (n bp) on the exit side. The FRET values of the nucleosome population with a single donor dye on the H2A subunit proximal to the acceptor dye are presented here. The FRET distributions of the n = -3, 3, 6, 8, 10, 11, and 13 bp nucleosomes show resolvable peaks for the different donor-labeling configurations, and the peak with the highest FRET value is selected in each case. For the n = 18 bp nucleosome, all donor-labeling configurations yield very low FRET values that merged into a single peak, the value of which is used here. Except for the first point near 100% FRET and the last point near zero FRET where the FRET values should saturate, the FRET values can be approximated by a linear dependence on the linker length with a slope of -0.059 ± 0.002 (black line). A similar distance dependence was observed previously, with a small difference in the slope due to slight differences in the transmission properties of the emission filters used (Blosser et al., 2009). The deviation from the expected nonlinear distance dependence of FRET is due to the flexible linkers connecting the dyes to the DNA or nucleosome, which substantially broaden the distance dependence of FRET and make it largely linear over a large distance range (Blosser et al., 2009). Data are shown as the mean ± SEM (N = 250 - 400 nucleosomes).

(E) The initial FRET values (black symbols) and final FRET values after remodeling by ISW2 (red symbols) for nucleosomes with a ssDNA gap m bp from the SHL2 site. The linear fit (red

line) of the post-remodeling FRET values yields a slope of -0.059 ± 0.002, identical to that of the dependence of FRET on the preset exit DNA linker length as shown in (D). The FRET values of the nucleosome population with a single donor dye on the H2A subunit proximal to the acceptor dye are presented here. The FRET distributions of all constructs show well-resolved peaks for the different donor-labeling configurations, and the peak with the highest FRET value is selected in each case. Data are shown as the mean ± SEM (N = 250 - 400 nucleosomes).

In this work, we used the original Widom numbering system to define the *n* and *m* values (Lowary and Widom, 1998). Based on recent crystal structures of nucleosomes constructed with the 601 sequence (Chua et al., 2012; Makde et al., 2010; Vasudevan et al., 2010), all *n* values would increase by 1 bp because the nucleosome core particle contains only 145 bp instead of 147 bp of DNA. Therefore the linker DNA length on each side of the nucleosome would increase by 1 bp. However, since we only measure translocation distances, i.e. changes in *n* rather than the absolute values of *n*, the conclusions drawn in this work do not depend on which numbering system is used. The *m* values, i.e. the distance between the ssDNA gap and the SHL2 site, remain the same independent of which numbering system is used.

Figure S2. Exit-side DNA translocation during remodeling by different ISWI-family enzymes, related to Figure 2.

(A-C) Exit-side DNA translocation of the n = 3 bp or n = -3 bp nucleosomes by ISW2 (A), ISW1b (B) and Isw2p (C). Shown are histograms of the FRET values during the entire remodeling course constructed from n = 3 bp (left) and n = -3 bp (right) nucleosomes. The histograms were constructed from the FRET time traces during the time window that starts when

the FRET value begins to decrease and ends when the FRET value begins to level off at near zero. Numbers above double-headed arrows shown in the histograms represent mean step sizes.
(D, E) The distributions of FRET values at direction-reversal points during remodeling by Isw2p (D) and ISW1b (E). The numbers above the peaks indicate the total translocation distances before direction reversal. The lowest peak in (E) is too close to zero to allow accurate calculation of the translocation distance because FRET saturates at zero for large donor-acceptor distances.

Figure S3. Observation of 1-bp DNA translocation steps at the exit side of nucleosomes in the presence of ATP-γ-S or at 15°C, related to Figure 3.

(A) Left: A representative experimental FRET time trace (blue) fit by either a hidden Markov modeling (HMM) algorithm (McKinney et al., 2006) (red) or a step-finding algorithm (Kerssemakers et al., 2006) (green). The FRET trace is the same as shown in Figure 3C.
Right: Histograms of FRET plateaus determined using the step-finding algorithm (Kerssemakers et al., 2006). Although the step-finding fit was performed on the entire FRET trace in this case, in the presentation of the distribution of FRET plateau values, we still divided the distribution into two FRET regions as in the case of the HMM analysis for comparison. Numbers above double-headed arrows represent mean step sizes. The peak positions and step sizes shown here are quantitatively similar to those derived using the HMM algorithm (McKinney et al., 2006), which are shown in Figure 3D.
(B) Left: FRET time trace, before (grey) and after (blue) 5-point averaging, of a single n = 3 bp nucleosome in the presence of 6.2 nM ISW2 and 2 μM ATP, recorded at 15°C. The red line shows the fit by the HMM algorithm.

Right: The distribution of FRET plateaus obtained from FRET traces recorded at 15°C determined using the HMM algorithm. Numbers above double-headed arrows represent mean step sizes.

Figure S4. Dependence of the dwell times associated with individual 1-bp steps on the concentrations of ATP and ATP-γ-S, related to Figure 4.

The pause number *k* denotes the FRET plateau after *k* bp of DNA translocation from the initial position for the *n* = 3 bp nucleosomes remodeled by ISW2.

(A) Dependence of the dwell times on the concentration of ATP-γ-S at a constant ATP concentration of 2 μM. The asterisks indicate dwell times that could not be directly observed in FRET traces in the absence of ATP-γ-S. At subsaturating ATP-γ-S concentrations, the 7^{th} pause is substantially longer than the dwell times associated with the other steps. The neighboring pauses (6^{th} and 8^{th}) also appear to be somewhat longer than the remaining pauses, most likely due to errors in pause identification. As the concentration of ATP-γ-S increases, the duration of the 7^{th} pause decreases while the durations of the other pauses increase.

(B) Dependence of the dwell times on the concentration of ATP at a saturating ATP-γ-S concentration of 2 mM. At saturating ATP-γ-S concentrations, all pauses have approximately the same duration that decreases with increasing ATP concentration.

Data are shown as the mean ± SEM (*N* = 15 - 25 events).

Figure S5. FRET distributions of entry-side-labeled nucleosomes before and after remodeling by ISW2, related to Figure 5.

(A) The initial FRET distribution of the nucleosomes before addition of the enzyme (blue bars). The black line shows the Gaussian fit. The FRET acceptor dye is 10 bp from the entry edge of the nucleosome. The FRET donor dye is attached to H2A. The nucleosome population with two donor dyes was removed by eliminating FRET traces with two donor-photobleaching steps. Hence the FRET distribution exhibits only two peaks (centered at FRET = 0.62 or 0.39), with the higher peak corresponding to the labeling configuration with a single donor dye on the proximal H2A subunit and the lower peak corresponding to the labeling configuration with a single donor dye on the distal H2A subunit.

(B) The FRET distributions of the nucleosomes upon addition of ISW2 alone (red line) or upon addition of both ISW2 and ATP (black shaded bars) superimposed on the initial FRET histogram (blue bars). After remodeling, the acceptor dye is moved into the nucleosome and should be within FRET range to both donor dye positions. Because the remodeled nucleosomes may not be centered on DNA exactly, the FRET distribution after remodeling is relatively broad.

Figure S6. Comparison of t_{wait} for nucleosomes with and without a ssDNA gap and exit-side translocation time traces for nucleosomes with a ssDNA gap., related to Figure 6

(A) The waiting times t_{wait} before the onset of remodeling activity measured at entry (yellow bars) and exit side (purple bars) of nucleosomes with (solid bars) or without (patterned bars) a ssDNA gap at m = 10 bp from the SHL2 site, which allows for only 10 bp of DNA translocation to the exit side. The ATP concentration is 2 μM. Data are shown as the mean ± SEM (N = 40 - 100 events).

(B) Example FRET time traces of the exit-side-labeled nucleosomes with a ssDNA gap at m = 5 bp (left) and m = 10 bp (right).

EXTENDED EXPERIMENTAL PROCEDURES

Preparation of dye-labeled mononucleosomes

Double-stranded dye-labeled DNA constructs were created by PCR (constructs with exit-side dye labeling) or by first annealing, then ligating a set of overlapping, complementary oligonucleotides (constructs with entry-side dye and/or 2-nt ssDNA gaps). 5'-Cy5 (exit-side dye) with a flexible linker was incorporated synthetically into oligonucleotides (Integrated DNA Technologies) used as PCR primers. For internal Cy5 labeling (entry-side), an oligonucleotide containing an internal Cy5 dye was directly incorporated into the backbone. Histone H2A protein was specifically labeled on a unique cysteine (residue 120) with the donor Cy3 dye (GE Healthcare) (Blosser et al., 2009; Yang et al., 2006). Cy3-labeled and unlabeled H2A were mixed with other histone proteins (H2B, H3, and H4) to generate histone octamers. Mononucleosomes were reconstituted from DNA and H2A-labeled histone octamers by salt dialysis and purified by gradient ultracentrifugation (Luger et al., 1997).

Preparation of ISW2, Isw2p, and ISW1b

The ISW2 complex was purified from *Saccharomyces cerevisiae* strain BY4742, bearing two copies of FLAG epitope tag at the 3' end of the *ISW2* gene. The complex was affinity-purified as previously described (Tsukiyama et al., 1999) using anti-FLAG M2 agarose beads (Sigma) and subsequently FLAG peptides at a concentration of 1 mg ml^{-1} concentration for elution. Protein concentrations were determined by analyzing samples on a 4–20% gradient SDS–PAGE, stained with SYPRO Ruby protein gel stain (Molecular Probes), and comparing to bovine serum albumin (BSA) standards of known concentrations. *Saccharomyces cerevisiae* strain YTT449,

with a FLAG epitope-tagged version of *ISW1*, was used to purify ISW1b, essentially as described previously (Gangaraju and Bartholomew, 2007). Briefly, the ISW1a and ISW1b complexes were separated by cation exchange chromatography (BioRex-70 resin) using a linear NaCl gradient (0.2-0.8 M). Fractions containing ISW1b were pooled and further purified by immunoaffinity chromatography with FLAG M2 beads. Elutions were analyzed on a 4-20% gradient SDS-PAGE, stained with colloidal blue (Pro-Blue; OWL Separation Systems), and quantified using known amounts of BSA protein as standards.

Automated determination of the durations of translocation phases (t_1 and t_2)

In order to determine the durations of the translocation phases, traces were subjected to a 2-5 point median filter. In each trace and for each translocation phase, a time point clearly before the start or clearly after the end of the translocation phase was interactively set as the initial guess of the starting or ending point for the following automated procedure. A running standard deviation was calculated for a set of consecutive, overlapping time windows moving in the direction of increasing time from the initial guess of the starting point or in the direction of decreasing time from the initial guess of the ending point. When this standard deviation value exceeded a threshold value (0.02), the center point of the current time window was recorded as the final starting or ending point of the translocation phase. The duration was calculated as the time difference between the ending and starting points of each translocation phase.

Automated step identification using two algorithms

The remodeling FRET traces were fit with a HMM algorithm (McKinney et al., 2006) (http://bio.physics.illinois.edu/HaMMy.html) or an alternative step-finding algorithm

(Kerssemakers et al., 2006). For HMM analysis, FRET time traces were divided into a low FRET ($0.32 \leq \text{FRET} \leq 0.62$) and a high FRET ($0.59 \leq \text{FRET} \leq 1$) segment. Each segment of every trace was individually fit, but no input parameters were used for the fit except for the maximum allowed number (10) of distinct FRET states supported by the algorithm. The initial values of the 10 states were set to be equally spaced within each of the two segments in all cases. The final number of the populated FRET plateaus identified in each of the two segments was substantially smaller than 10 (typically only 4-5), allowing for an unbiased analysis of the distinct FRET states.

To determine the fraction of steps that could be detected in FRET traces using this HMM analysis, we simulated traces using a preset number of 1-bp steps, an exponential distribution of the dwell times of the steps with an experimentally determined stepping rate, and the experimentally determined signal-to-noise ratio in FRET. Analysis of these simulated traces with the HMM algorithm showed that approximately 50% of the 1-bp steps within the dynamic range were identified, while the remaining plateaus evaded detection primarily due to their short dwell times.

As an alternative to the HMM algorithm we also applied a step-finding algorithm developed by (Kerssemakers et al., 2006) to fit the remodeling time traces with a staircase function. Here no *a priori* assumption about the number of steps is made. Instead, this number is chosen such that it maximizes a figure of merit ('step-indicator' S) (Kerssemakers et al., 2006). The fits obtained using this algorithm were quantitatively similar to those obtained from the HMM algorithm.

Supplemental Figure

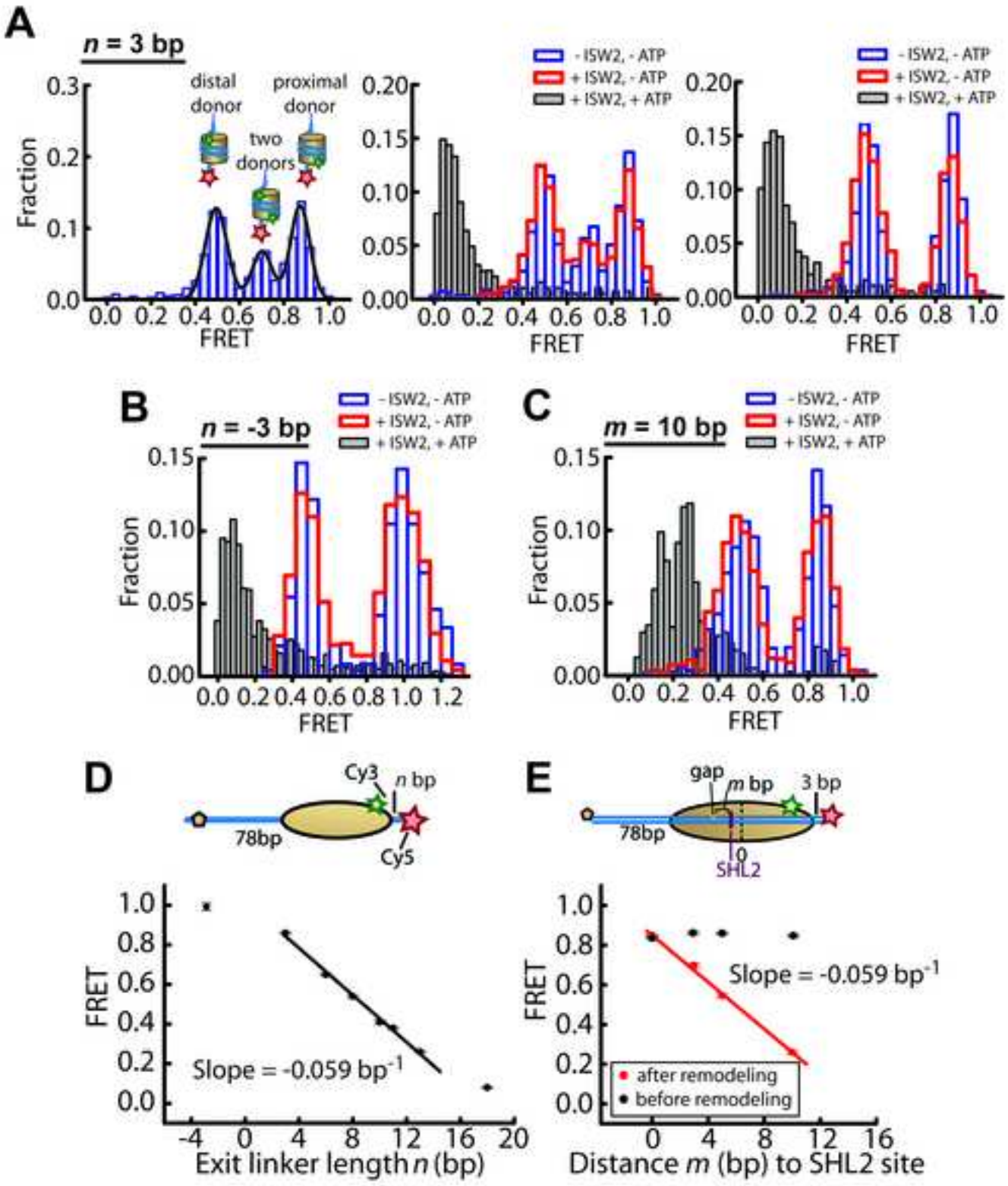

Figure S1, Deindl et *al.*

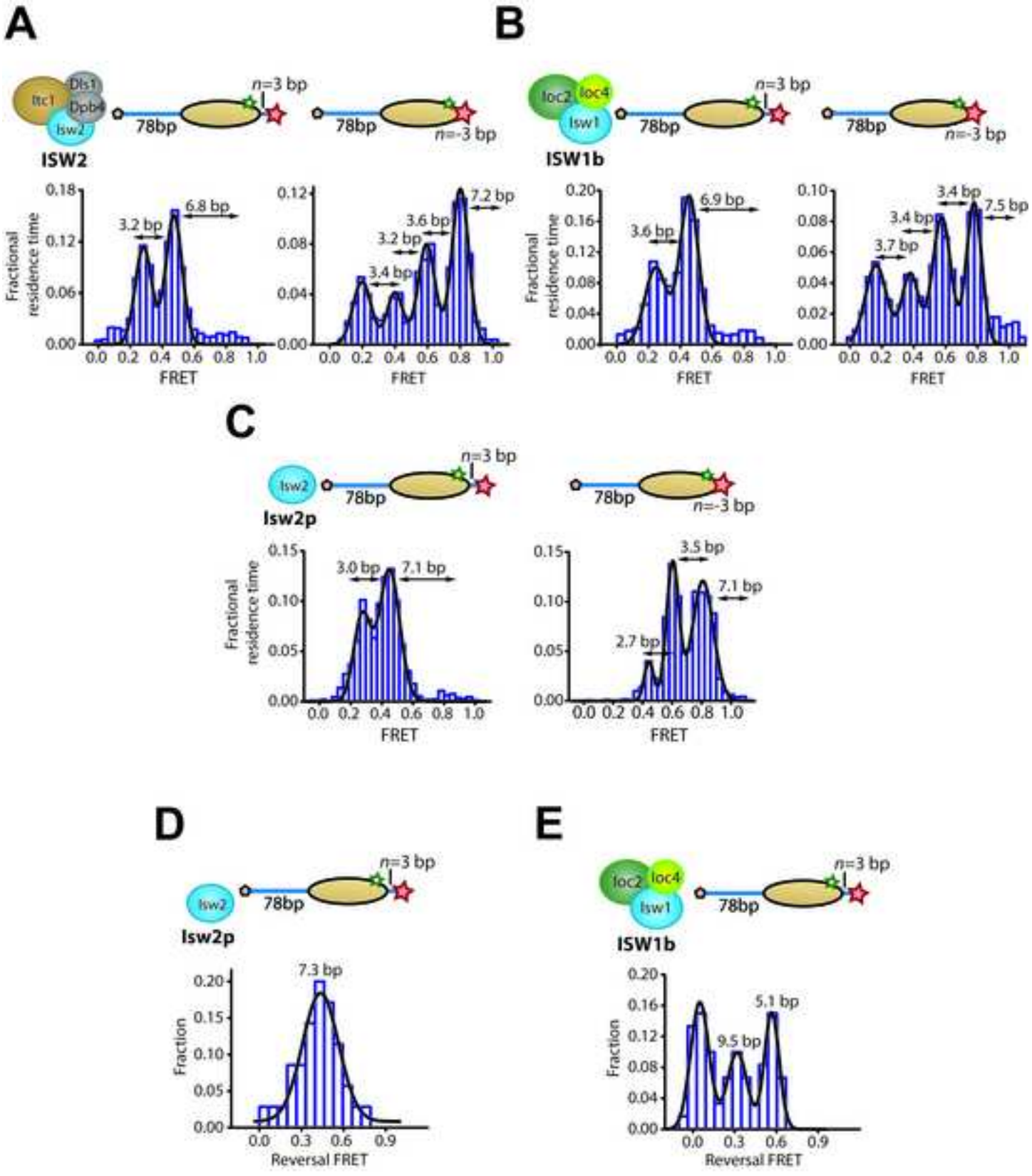

Figure S2, Deindl et *al.*

Supplemental Figure

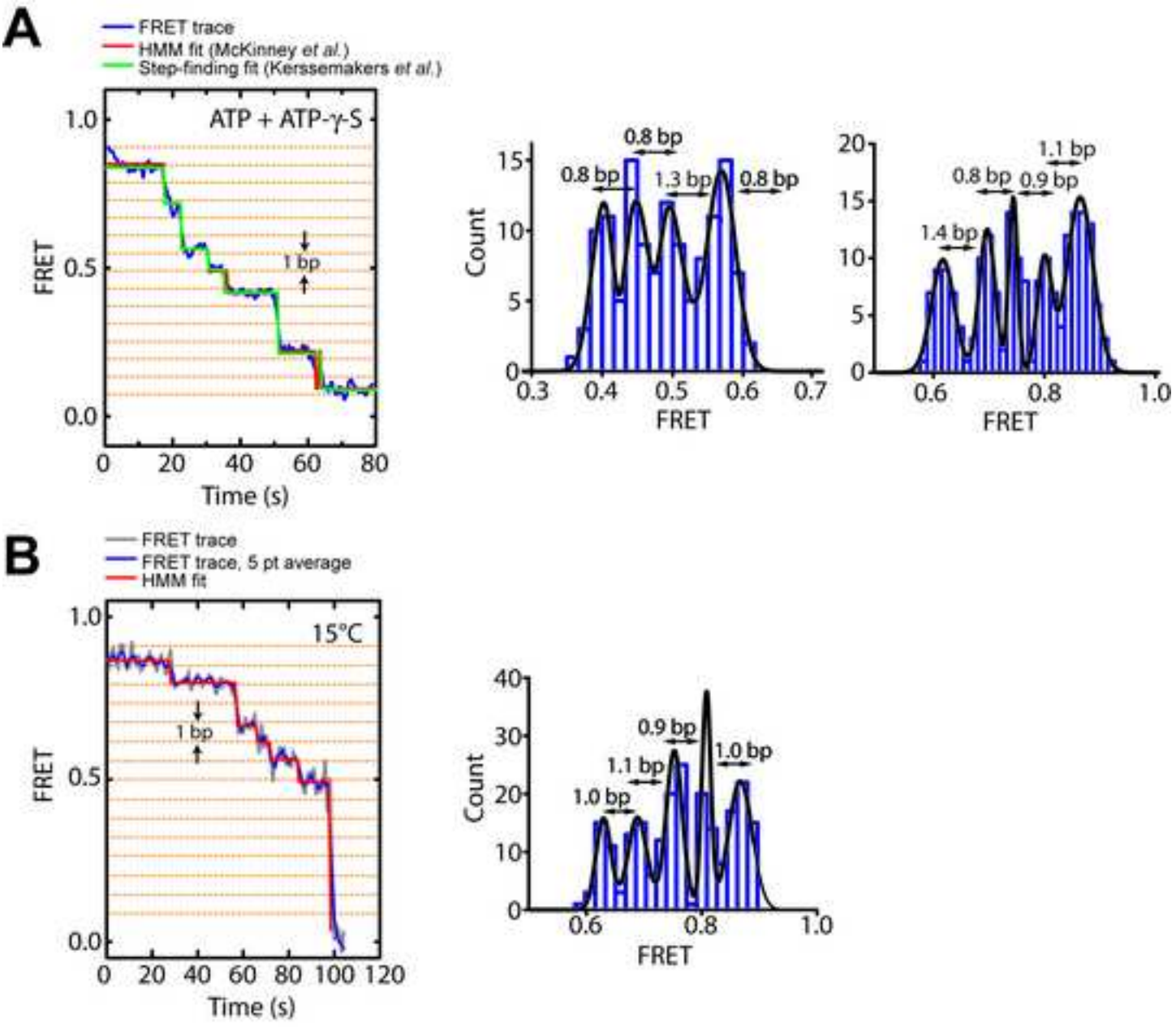

Figure S3, Deindl et *al.*

Supplemental Figure

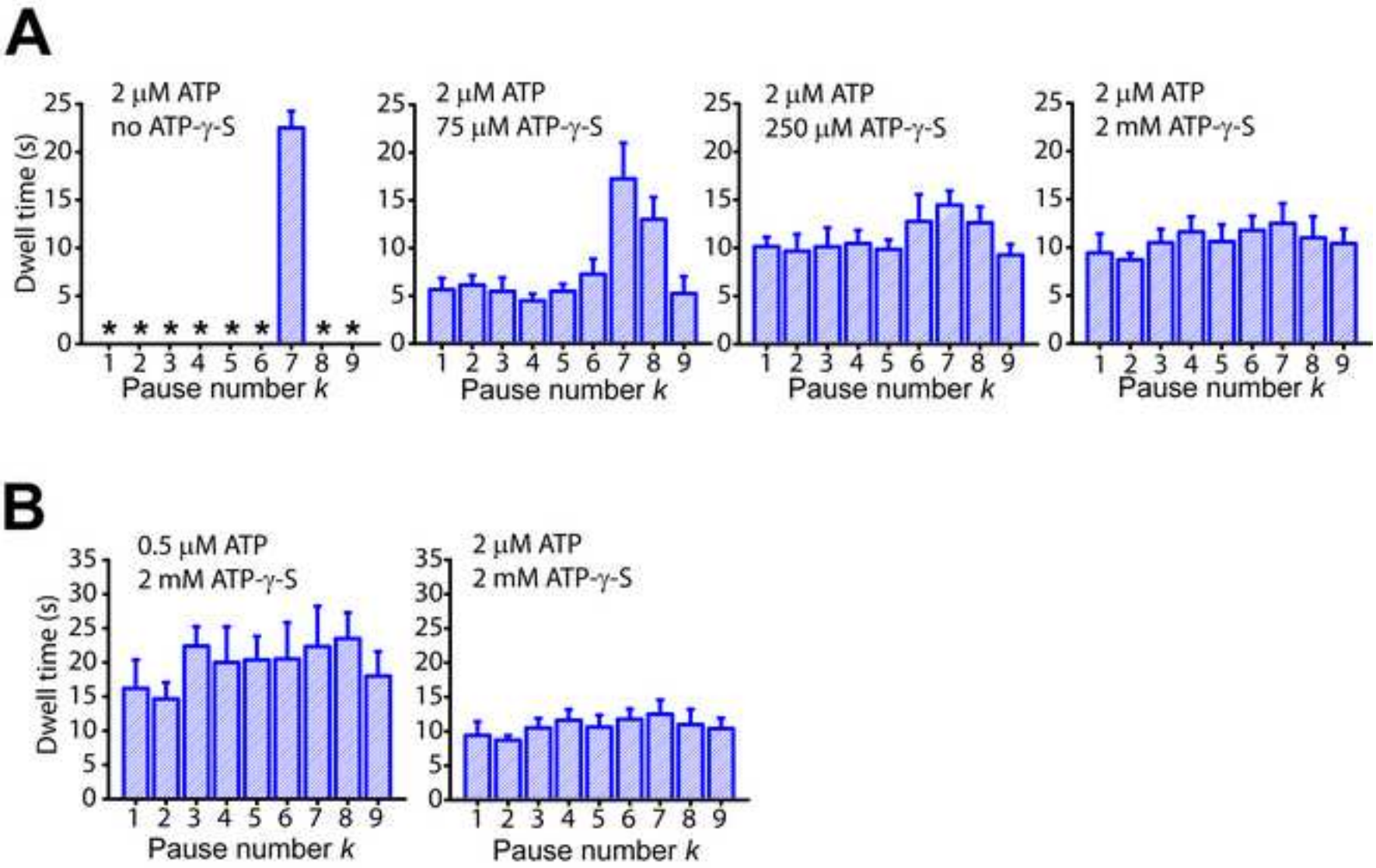

Figure S4, Deindl et *al.*

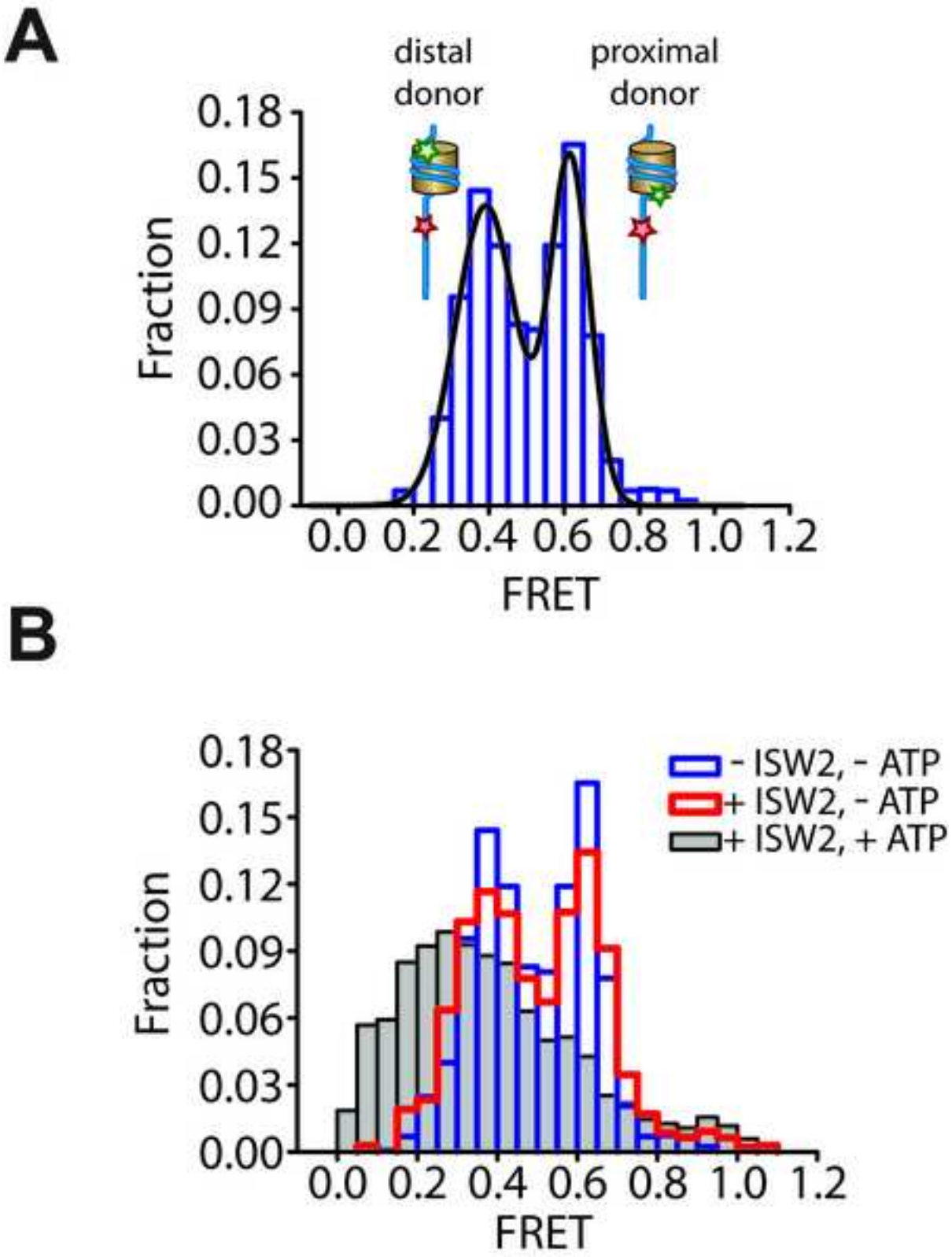

Figure S5, Deindl et *al.*

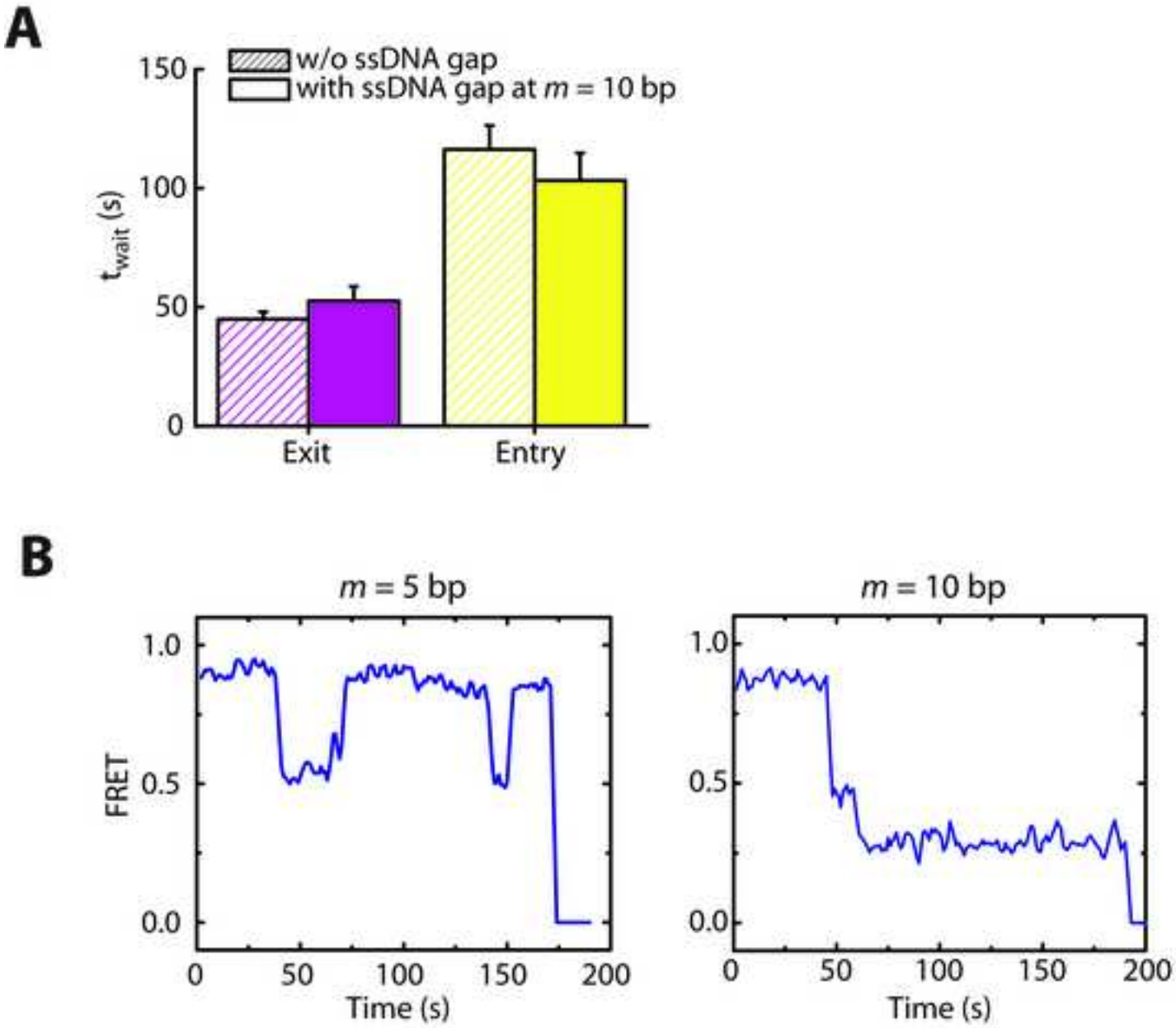

Figure S6, Deindl et *al.*